

Study on the mechanism of the difference in flotation performance between fine-grained crystalline SiO₂ and amorphous SiO₂

Saisai Ma¹, Jie Li², Yonglun Wang¹, Bangqi Wei¹

¹School of Mining and Coal, Inner Mongolia University of Science and Technology, Baotou, China

²School of Materials and Metallurgy, Inner Mongolia University of Science and Technology, Baotou, China

Corresponding author: yjslijie@sohu.com (Jie Li)

Abstract: Numerous minerals found in nature contain silica, including quartz, cristobalite, opal, etc. They have the same chemical composition but different crystal structures, and this phenomenon is called “polymorphism” in mineralogy. For these polymorphic and multi-like minerals, in the flotation process, will it directly or indirectly affect the flotation effect. Based on this, this study mainly explores the difference between crystalline SiO₂ and amorphous SiO₂ in flotation. In this study, two crystal forms of SiO₂ were subjected to flotation and adsorption capacity tests. FTIR, other test techniques, the chemical calculation of the flotation solution, and the theoretical calculation of the DLVO can all be used to provide an explanation. Finally, in the flotation experiment, the feedbacks of the two minerals to the change of the pH value of the pulp and the change of the concentration of the reagent are different. Through the comprehensive analysis of the adsorption capacity test and semi-quantitative calculation of the infrared spectrum, the adsorption capacity of crystalline SiO₂ to drugs is about 23% higher than amorphous SiO₂. Furthermore, during the flotation process, the amorphous SiO₂ particles will agglomerate together and entrain into the foam through, resulting in concentrate pollution. So amorphous SiO₂ will undoubtedly increase the difficulty of flotation.

Keywords: flotation separation, heteromorphism, infrared spectrum calculation, DLVO theory

1. Introduction

Quartz group minerals are the most abundant minerals in nature (Shi and Zhang, 2017; Zhou, 2015). In addition to common quartz, there are many other forms, such as SiO₂ in α -cristobalite, a cubic crystal structure, tridymite, except for crystalline SiO₂ minerals. There is also amorphous opal, and silica can be found in solid waste in various industries. For example, silica as by-product of ferrosilicon “silica fume” also exists in amorphous form. The diversity of the silicon-oxygen tetrahedron combination forms different crystal structures, which become the phenomenon of homogeneity and polymorphism (Zhou et al., 2015). With the passage of time and the continuous mining of minerals, the high-quality mineral resources that are easy to mine and select are decreasing, and the remaining mineral resources are “poor, fine, and miscellaneous,” gradually becoming the main theme (Abaker and Aslan, 2023). Flotation method is more adaptable to fine-grained minerals.

There is limited information on the flotation of amorphous SiO₂, and flotation is rarely used to treat silica minerals in an amorphous state. The more uneven the surface, the better the floatability (Griffiths and de Haset, 2006). The crystal quartz surface is anisotropic. This assertion leads to the assumption that amorphous SiO₂ should have a lower floatability than quartz. Li et al. (2021) used flotation and nanobubble technology to purify amorphous microsilica fume, which can enrich extremely fine microsilica powder into foam, and eventually achieved a silicon grade of more than 80%. Furthermore, in the study on the rheology of slurry, Chen et al. (2017) found that amorphous SiO₂ would enhance the viscosity of pulp. During positive flotation of copper ore, amorphous SiO₂ easily entered the concentrate, lowering the concentrate grade. Zhu et al., (2020) especially focused on the influence of quartz surface roughness on the flotation effect. Quartz obtained by different crushing and grinding

machinery have different chemicals adsorption capacities. Quartz with larger surface roughness can adsorb more chemicals. Zhou et al. (2015) used the simulation method to summarize the differences in the surface structure and hydration properties of silica homogenous polymorphic minerals (α -quartz and α -cristobalite) as well as the hydroxyl types and hydration characteristics on different crystal surfaces of quartz. The densities are all different. Quartz is easier to combine to form a hydrogen bond network compared with cristobalite. Martínez-Carrillo and Uribe-Salas (2008) examined the empirical entrainment model proposed by earlier researchers in the article, and his group conduct flotation tests on fine SiO_2 powder in a flotation column to develop a new estimate of mechanical entrainment. The model was used to comprehensively investigate the effects of hydrophilic solid content, foam depth, and superficial air velocity on the entrainment degree in the feed. The typical hydrophilic material SiO_2 also exhibits the entrainment phenomena. Whether the degree of entrainment is related to the crystal structure is worthy of our study. Therefore, a comparative experimental study on the flotation performance of amorphous SiO_2 and crystalline SiO_2 was performed in this paper. In this study, the difference between crystalline SiO_2 and amorphous SiO_2 under the same flotation test conditions, the difference in the adsorption of flotation reagents, as well as the difference in the surface properties of the two SiO_2 were investigated (Hu et al., 2007).

This study has a certain guiding significance in the future to optimize the flotation process and reduce the influence of mechanical entrainment when separating amorphous SiO_2 minerals. Additionally, more researchers are beginning their studies on the impact of mineral crystal structure on the flotation process from the perspective of the crystal structure of the mineral. Additionally, novel techniques for the flotation separation of amorphous minerals and the optimization of mineral flotation processes can be developed with the development of first-principles calculation and simulation technologies. The flotation process is now better equipped to handle amorphous and fine-grained minerals in the future.

2. Materials and methods

2.1. Materials

The crystalline SiO_2 and amorphous SiO_2 used in this experiment was taken from a company in Lianyungang City, Jiangsu Province. Sieve 200~400 mesh particle(-0.074mm~+0.038mm). The X-ray diffraction spectrum X-ray fluorescence spectrum and BET were used to test the two samples, respectively. The test results are shown in Table 1, Table 2, Table 3 and Fig. 1 below.

Table 1. XRF results of crystalline quartz SiO_2

| element | SiO_2 | Al_2O_3 | Fe_2O_3 | CaO | BaO | Cr_2O_3 |
|---------|----------------|-------------------------|-------------------------|-------|-------|-------------------------|
| wt% | 98.678 | 0.085 | 0.066 | 0.023 | 0.024 | 0.008 |

Table 2. XRF results of amorphous SiO_2

| element | SiO_2 | Al_2O_3 | Fe_2O_3 | CaO | BaO | Cr_2O_3 |
|---------|----------------|-------------------------|-------------------------|-------|-------|-------------------------|
| wt% | 99.097 | 0.067 | 0.059 | 0.043 | 0.024 | 0.009 |

Table 3. Specific surface area results of crystalline quartz SiO_2 and amorphous SiO_2 .

| Form | Specific surface area (m^2/g) |
|----------------------------|---|
| Crystalline SiO_2 | 0.6852 |
| Amorphous SiO_2 | 0.7519 |

It can be clearly seen from the results of the X-ray diffraction spectrum that sample 1 is SiO_2 in crystal form. Sample 2 has no diffraction peaks and appears as a diffuse "amorphous packet" Wang et al., 2002). Therefore, sample 2 is amorphous SiO_2 . The X-ray fluorescence spectrum test results show that the Si

content in the two SiO₂ samples is 98.678% and 99.097%, respectively. All meet the requirements of pure minerals as flotation test.

The Dodecylamine (DDA) agent used in the test was obtained from Aladdin Chemical Reagent Factory. The NaOH and HCl reagents are Longxi Chemical and Beijing Chemical Reagent Factory, respectively. Congo red indicator and sodium acetate are both from Tianjin Chemical Reagent Factory. The water used in the experiment was deionized water.

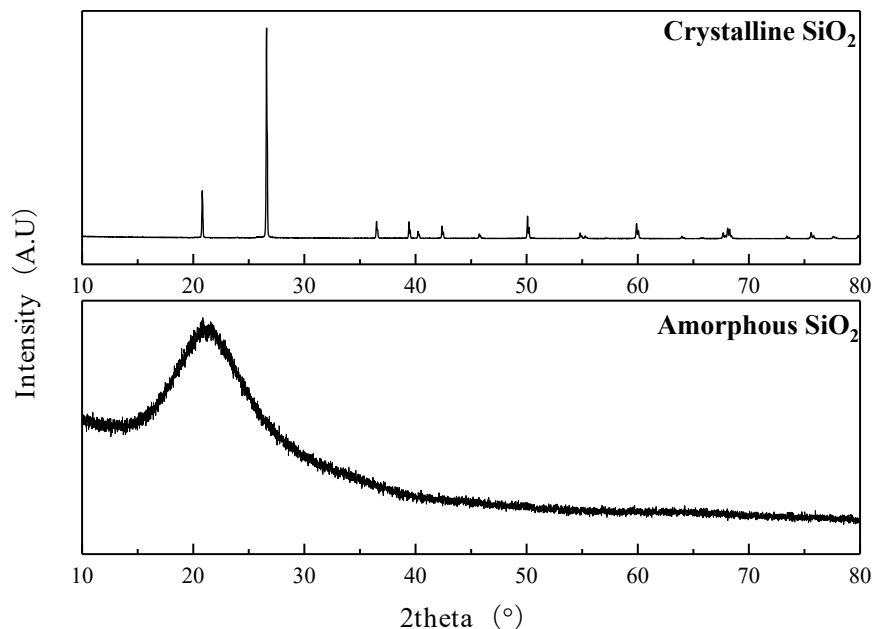


Fig. 1. X-ray diffraction spectrum

2.2. Methods

2.1.1. Flotation test

Adopt XFG hanging tank flotation machine (Jilin Prospecting Plant). The flotation cell capacity is 50 ml. The pulp concentration was determined to be 10%. The mechanical parameters of the flotation machine: the rotation speed is 1992 r/min, and the aeration volume is 0.6 m³/(m² min). The experiment adopted manual foam scraping, and the specified foam scraping time was 3 min. The flotation concentrates and tailings were filtered separately, dried at 40°C, and weighed, and the yield was calculated to represent the recovery rate.

2.1.2. Adsorption capacity test

A spectrophotometric technique for finding amine collectors was mentioned in the experiment (Liu et al., . The absorbance of deionized water was subtracted from different concentrations of amine collectors, acetate buffer solution (pH = 5), and Congo red solution. The standard curve equation was established by taking the absorbance as the ordinate and the amine concentration as the abscissa.

During the detection process, the sample to be tested was first added to the acetate buffer solution to adjust the pH to 5, then the Congo red solution with the concentration of 5×10^{-4} mol/L was added and deionized water was allowed to settle to the desired volume. The desired mixed solution is attained. To evaluate the sample's absorbance, combine the test sample, the Congo red solution, and the test mixture in a ratio of 5:2:25 and set it in an ultraviolet spectrophotometer at a wavelength of 490–497 nm. The concentration of the remaining DDA collector in the pulp is determine using the standard curve equation, and finally obtain the collector content adsorbed on each gram of SiO₂.

2.1.3. Zeta potential test

A 0.2000 g sample of the raw material used in the test was precisely weighed and thoroughly milled to a thickness of $-5 \mu\text{m}$. To adjust pH, prepare a 100 ml suspension and add HCl or NaOH. Aspirate the

supernatant after letting stand for 5 min. A Zeta potential meter detected the Zeta potential value (Brookhaven Zeta Plus).

2.1.4. FTIR test

Infrared spectroscopy was performed on two SiO₂ pure mineral samples and the samples after flotation reagents. The sample and spectrally pure potassium bromide are thoroughly mixed in 1:150 and pressed into tablets to prepare positive potassium bromide carrier sheets. Fourier transform infrared spectrometer (Bruker VERTEX 70) was used for detection. The infrared spectrum measurement range is 400-4000 cm⁻¹. Based on Beer's formula, infrared spectroscopy's semi-quantitative analysis determines that the absorbance is proportional to the material content (Griffiths and de Haseth, 2006; Weng, 2010). In order to determine the absorption peak area and the second derivative spectrum, the software is also utilized to fit a specific infrared absorption peak. Peak area changes are compared to substance content changes (Wu et al., 2021).

2.1.5. Flotation solution stoichiometry

The concentration of the flotation agent DDA's dissociated components in the pulp was determined using the tracing method (Wang, 1988; Hu and Li, 1990). And draw the relationship between the concentration of dissociated components and the pH value of the pulp, that is, the lgC-pH diagram. With the help of this Fig., it is possible to explain the active components of DDA that play a dominant role in different pulp pH environments.

2.1.6. DLVO theoretical analysis

According to the classical DLVO theory, whether a sol can exist stably under certain conditions depends on the potential energy of the interaction between the colloidal particles. The total potential energy equals the sum of the van der Waals attraction potential energy and the electrostatic repulsion potential energy caused by the electric double layer (Hu et al., 2021). Based on this theory, the total potential energy of the two slurry systems can be calculated, and the anti-agglomeration ability between the particles of the two minerals in the flotation process can be predicted.

3. Results and discussion

3.1. Flotation test results

3.1.1. Influence of pulp pH value on the recovery rate of two kinds of SiO₂ flotation

In this test, DDA was used as the collector at a concentration of 4×10^{-4} mol/L. The pH was increased sequentially, and the pH adjusting agent used HCl and NaOH solution. Fig. 2 shows the flotation recovery rates of the two at different pH.

The experiment found that the pH change had a certain influence on the flotation results of the two. The feedback to pH maintained a similar trend for both samples across the pH environment. Under neutral and weak alkaline conditions, high recovery rates were maintained.

Under acidic conditions, the flotation effect of DDA was slightly worse and kept below 50%. The flotation effect of amorphous SiO₂ is better than that of crystalline SiO₂. In the neutral range of pulp, the flotation recovery rates of amorphous SiO₂ and crystalline SiO₂ are quite different. Crystal quartz SiO₂ has the best flotation effect at pH = 7; the flotation recovery rate is 91%. In contrast, the flotation recovery of amorphous SiO₂ at pH = 8 reached the maximum value of 92%. When the pH was greater than the optimum, the flotation recovery rates both began to decline. At pH = 12, the recovery rate dropped to 50%-60%.

From the overall test results, for the pH change feedback, the amorphous SiO₂ exhibits a "hysteresis" relative to the crystalline SiO₂.

3.1.2. Effect of collector concentration on recovery rates of two SiO₂ flotations

In the above experiments, it was found that crystalline SiO₂ and amorphous SiO₂ achieved the maximum flotation recovery at pH = 7 and pH = 8, respectively. Therefore, the pH conditions were fixed at 7 and

8, respectively, to explore the effect of the concentration of DDA on the flotation recovery rate. The test results are shown in the Fig. 3.

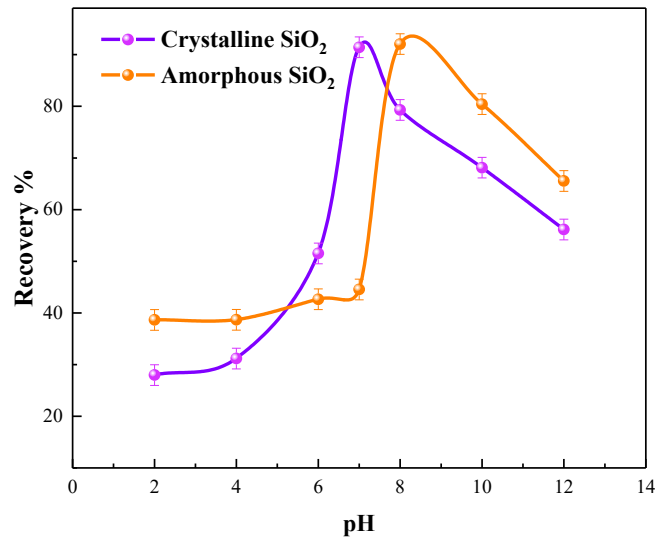


Fig. 2. Flotation recovery of both at different pH

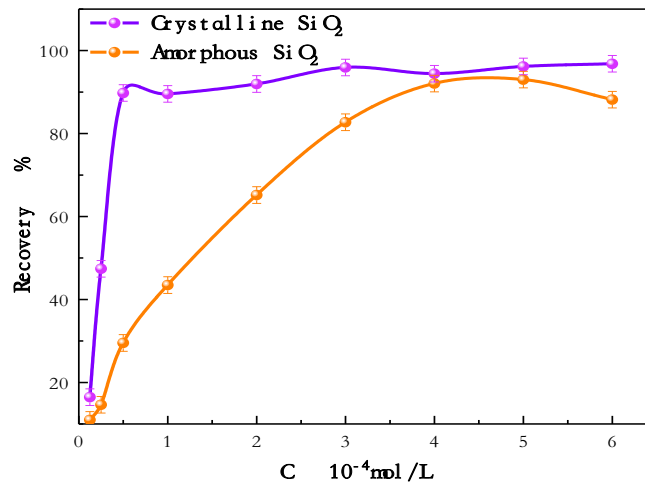


Fig. 3. Flotation recovery rates of the two under different collector concentrations

According to the test results in the above Fig., it can be observed. With the increase of the concentration of DDA, the flotation recovery rates of both SiO₂ showed a trend of first increasing and then remaining stable.

The flotation recovery rate of crystalline SiO₂ increased rapidly when the DDA concentration was in the range of 0.125–0.5 × 10⁻⁴ mol/L. The flotation recovery rate increased from 16.45% to 89.78%. The growth of amorphous SiO₂ in this concentration range is relatively slow, only 10.975% to 29.525%.

When the DDA concentration increased to 0.5 × 10⁻⁴ mol/L, the flotation recovery rate of crystalline SiO₂ stabilized above 90%, and no significant increase occurred. The flotation recovery rate of amorphous SiO₂ increased steadily with the increase of DDA concentration until the DDA concentration was 5.0 × 10⁻⁴ mol/L, the extreme value appeared and then began to decline.

The recovery of crystalline SiO₂ was significantly higher than that of amorphous SiO₂ at lower collector concentrations. In the low-concentration drug range, crystalline SiO₂ was more sensitive to changes in drug concentration. When the concentration of DDA was 0.5 × 10⁻⁴ mol/L, the recovery rate of crystalline SiO₂ can be stable at about 90%. On the contrary, amorphous SiO₂ needs a DDA concentration of 5 × 10⁻⁴ mol/L to stabilize the flotation effect. Regarding collectors concentration, amorphous SiO₂ flotation had the greater demand for chemicals and needs to consume more collectors.

3.2. Adsorption capacity test results

Absorbance was measured by a series of DDA solutions of known standard concentrations. After linear fitting, the standard curve equation was obtained, where $R^2 = 99.9635$. The Fig. 4 below shows the change in the adsorption amount of the two samples after the action of different concentrations of DDA.

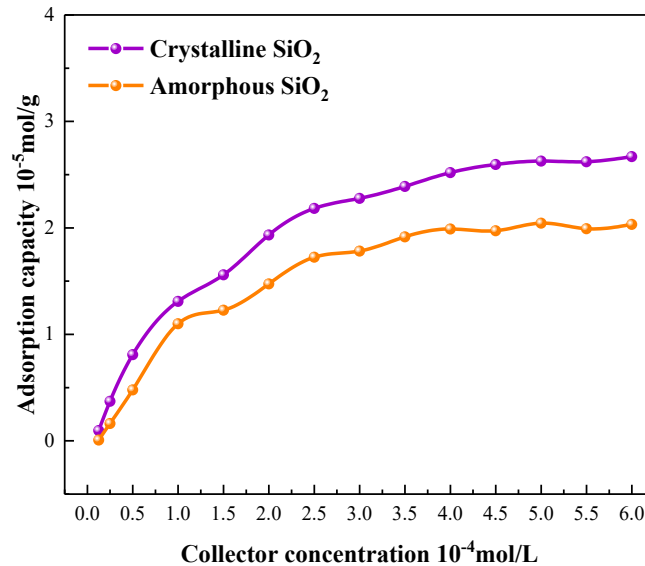


Fig. 4. Adsorption capacity at different collector concentrations

The above experimental research found that when the concentration of DDA is 5.0×10^{-4} mol/L, the flotation recovery rate of both can achieve the best flotation recovery rate. However, the adsorption of the agent on the surface of amorphous SiO_2 was 1.98934, and that of the crystal was 2.51965. The difference between the two is 21.047%. When the collector concentration is 4.5×10^{-4} mol/L, the maximum difference in adsorption capacity is 23.971%.

The adsorption methods in flotation can be roughly divided into chemical adsorption, adsorption formed by chemical bonds, and physical adsorption formed by physical forces, such as van der Waals force and electrostatic force. According to the literature (Martinez-Carrillo and Uribe-Salas, 2008; Cao et al., 2021; Wei et al., 2018; Lelis et al., 2022), the adsorption of DDA on the quartz surface is mainly physical. After the dissociation of DDA, the polar groups RNH_3^+ and $\text{RNH}_3^+-\text{RNH}_2$ associates are adsorbed on the surface of SiO_2 by electrostatic force, changing the wettability of the surface of SiO_2 , and making the surface of SiO_2 strong hydrophilicity become hydrophobic surface, and then float up with the bubbles.

The main effect of DDA on the surface of SiO_2 is electrostatic force. Therefore, the difference in adsorption performance between the two is mainly due to the electrical properties of the two surfaces. It can be speculated that the surface energy of amorphous SiO_2 is smaller than that of the crystal surface, and subsequent Zeta potential tests can verify this guess.

Under the same concentration, the dosage of DDA adsorbed on the surface of amorphous SiO_2 is lower than that of crystalline SiO_2 . At the concentration of 4.0×10^{-4} mol/L, the adsorption rate of the amorphous SiO_2 agent is 10% less than that of the crystalline SiO_2 agent. It is speculated that the maximum adsorption rate has been completed at 4.0×10^{-4} mol/L, and the flotation is effective when the concentration continues to increase. It may be due to foam layer entrainment and other reasons that the recovery rate of amorphous SiO_2 flotation continues to rise (Nykänen et al., 2018; Ye and Wang, 2018).

3.3. Mechanism analysis

3.3.1. Zeta potential analysis

Both samples were Zeta tested on pure minerals and after DDA. The test results are shown in Fig. 5. The Zeta potential test results showed slight differences in the Zeta potential of the two minerals with

the change in pH. The electronegativity of crystalline SiO₂ is slightly stronger than that of amorphous SiO₂, especially in the pH = 4–9 range.

The reason is analyzed: The crystal SiO₂ has a regular tetrahedral structure. When breaking, the lattice potential needs to be broken to expose the fracture surface. The exposed Si-O on the broken surface still maintains directional arrangement, and the surface contacts with water molecules and combines with them to generate Si-OH. Hydrogen bonds may be formed between adjacent silanol groups, and hydrogen bonds will also be formed between particles (Hu et al., 2007; Berro et al., 2020). However, due to the nature of crystal orientation, except for the hydrogen bonds between adjacent particles, the number of generated hydrogen bonds is the same. However, amorphous SiO₂ does not have the property of crystal orientation. The Si-O arrangement is intricate. The broken bonds exposed when broken will easily form hydrogen bonds after combining with water molecules, and the probability of generating hydrogen bonds is much greater than that of the crystalline SiO₂ structure. The decrease of surface negative charge holes is caused by the hydrogen bond structure.

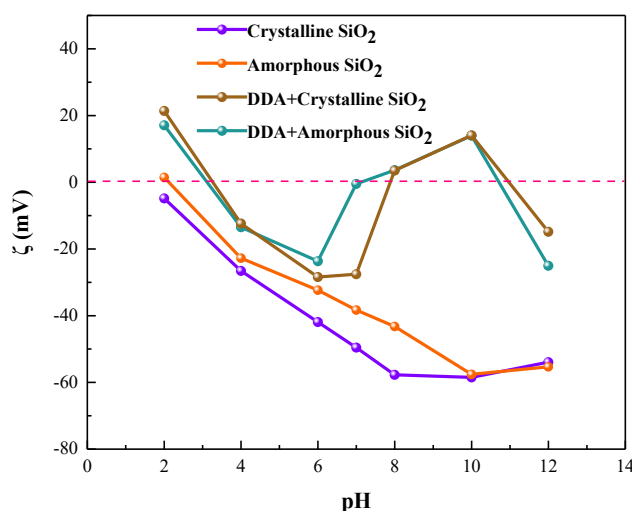


Fig. 5. Zeta potential diagram

After the addition of DDA, the potentiodynamic of both SiO₂ samples increased, which was mainly affected by the cationic group RNH₃⁺ dissociated from DDA. The potential of crystalline SiO₂ changes from negative to positive at pH=7, while that of amorphous SiO₂ at pH=8. After pH=6, the range of potential changes began to increase, which was consistent with the trend of flotation. It adsorbs on the surface of SiO₂ minerals and changes the electrical properties of the SiO₂ surface. The surface electronegativity of crystalline SiO₂ is still greater than that of amorphous SiO₂; that is, the effect of DDA on the surface of the two SiO₂ minerals is the same.

In addition, the system's stability can be predicted by the value of the Zeta potential on the surface of the mineral particles. The smaller the absolute value of Zeta potential, the more tendency of the system to agglomerate or agglomerate. From this, it can be speculated that the tendency of amorphous SiO₂ to agglomerate will be stronger.

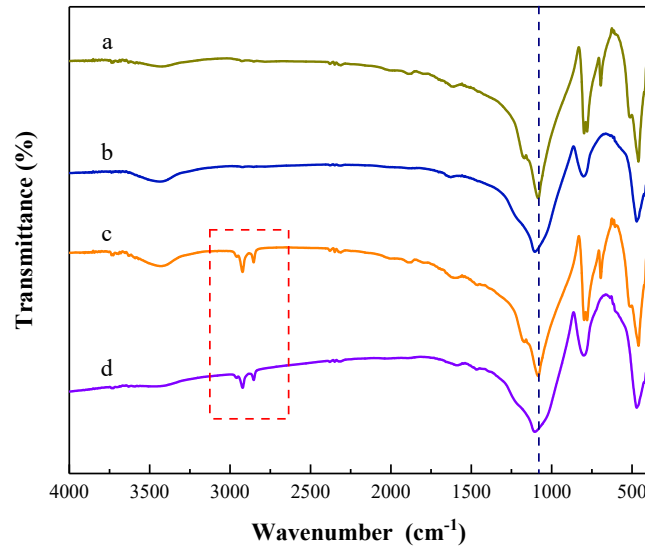
3.3.2. FTIR analysis

The Fourier infrared spectrum test was performed on the two SiO₂ before and after the action of DDA, and the infrared spectrum is shown in a- Crystalline SiO₂, b- Amorphous SiO₂, c- Crystalline SiO₂ treated with DDA, d-Amorphous SiO₂ treated with DDA

Fig. 6.

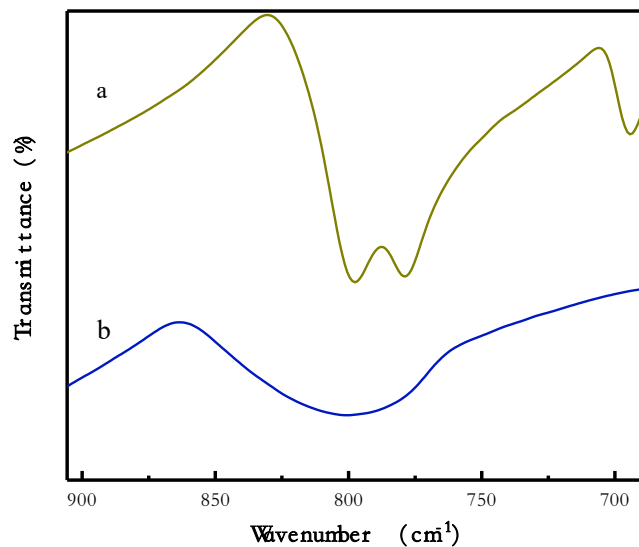
It can be seen from the infrared spectrum in Fig. 6 that a and b respectively test the infrared spectra of two SiO₂ samples. There are some subtle differences in the infrared spectrum between the two. Curve a is the infrared spectrum of crystalline SiO₂, near 1100 cm⁻¹, 1083cm⁻¹, 798 cm⁻¹,779 cm⁻¹and 459 cm⁻¹ is the characteristic absorption peak of Si-O-Si.

The shown in Fig. 7 below. In curve b, at 800 cm^{-1} , there is only one Si-O symmetrical stretching absorption peak, which is the biggest difference from crystalline quartz. According to Weng (2010), the absorption peak is the basis for distinguishing crystalline SiO_2 from amorphous SiO_2 . In addition, in the Si-O-Si antisymmetric stretching vibration absorption band in the 1100cm^{-1} , the absorption peak at 1174 cm^{-1} in amorphous SiO_2 disappears, and the absorption peak of Si-O-Si at 1105 cm^{-1} is red-shifted by 12 cm^{-1} .



a- Crystalline SiO_2 , b- Amorphous SiO_2 , c- Crystalline SiO_2 treated with DDA, d- Amorphous SiO_2 treated with DDA

Fig. 6. Infrared Spectrum



a- Crystalline SiO_2 , b- Amorphous SiO_2

Fig. 7. High-resolution infrared absorption spectrum

The infrared spectrum of crystalline $\text{SiO}_2 + \text{DDA}$ in curve c and curve d is different from the curve a and curve b in that new absorption peaks appear at 2853 cm^{-1} and 2992 cm^{-1} . The absorption peaks here are $-\text{CH}_3$ and $-\text{CH}_2-$ of the alky groups in the DDA agent. Therefore, DDA is adsorbed on the surface of crystalline SiO_2 and amorphous SiO_2 . In comprehensive curve a and curve b, the position of the absorption peak does not shift, which proves that the adsorption mode is physical adsorption (28).

From the intensity observation, the intensity of the peak of the crystalline SiO_2 adsorbing agent is slightly larger than that of the amorphous SiO_2 . To clearly distinguish the difference between the two.

Therefore, it is more intuitive to use the semi-quantitative calculation of infrared spectroscopy for quantitative comparison to show the difference in adsorption capacity between the two.

3.3.3. Quantitative calculation of infrared spectroscopy

Intercept the infrared spectrum in the range of 3000–2800 cm^{-1} . The amount of DDA adsorbed on the surfaces of the two minerals was compared using the semi-quantitative approach.

The calculation principle is based on Beer's law. When the thickness of the potassium bromide sheet is assured to be constant, the material content and absorbance are proportionate. Therefore, the content of the two substances can be compared according to the peak area of the absorption peak of the calculated absorbance spectrum (Wang et al., 2021).

Using OPUS infrared software, the infrared transmission spectra were converted into infrared absorption spectra, and the absorption spectra were normalized. The 3000–2800 cm^{-1} spectral part was intercepted to obtain a high-resolution smooth infrared absorption spectrum. The Fig. 8 below shows the high-resolution absorption spectrum in the 3000–2800 cm^{-1} wavenumber band. The peaks of the two spectra were fitted by Origin2017 software, and the peak areas were calculated. The fitting result graph is shown in 9, and the summary of the calculation results is shown in Table 4.

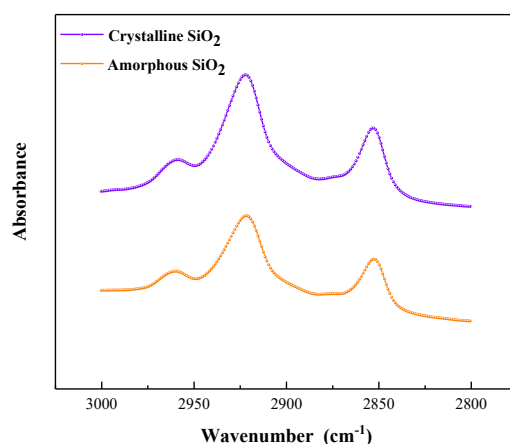


Fig. 8. High-resolution infrared absorption spectrum

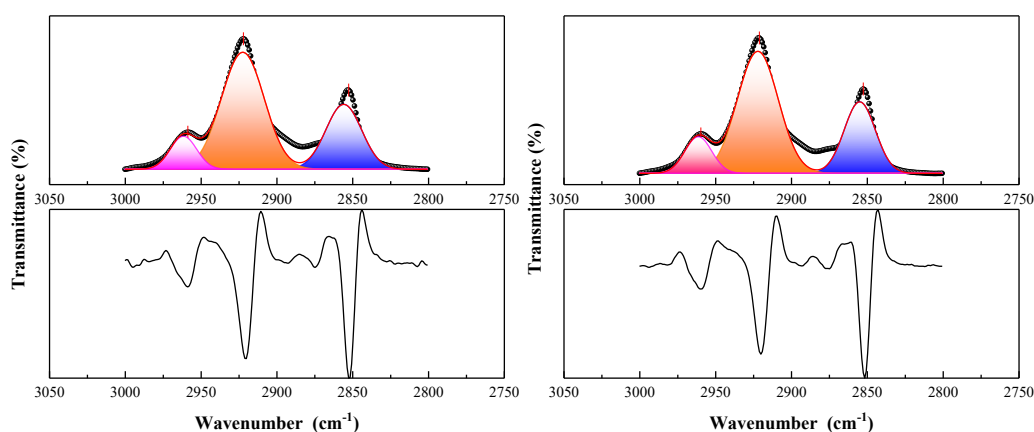


Fig. 9. Fitting diagram and second derivative of the drug absorption peak

Table 4. Infrared spectral fitting calculation results of two SiO_2 samples after the same concentration of DDA

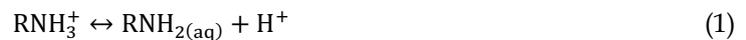
| Name | Peak position (cm^{-1}) | FWHM | Peak area | Total peak area |
|-------------------------------------|------------------------------------|--------|-----------|-----------------|
| Crystalline SiO_2 + DDA | 2961 | 20.572 | 1.25293 | 4.42468 |
| | 2922 | 33.272 | 2.70067 | |
| | 2855 | 27.816 | 0.47108 | |
| | 2961 | 20.950 | 0.37241 | |

| | | | | |
|------------------------|------|--------|---------|---------|
| Amorphous | 2922 | 31.747 | 2.18391 | 3.52646 |
| SiO ₂ + DDA | 2855 | 24.225 | 0.97014 | |

Through the absorption peak fitting calculation of the drug adsorption, it is found that under the same concentration of DDA, the peak areas of the adsorption peaks on the two SiO₂ surfaces are not the same. The adsorption on the crystalline SiO₂ surface was 20.300% more than that on the amorphous SiO₂ surface. The surface of crystalline SiO₂ has a stronger ability to adsorb chemicals, and the flotation recovery rate has stabilized at 90%–92% at this concentration. It can be shown that during the flotation process of amorphous SiO₂, many reagents remain in the pulp and cannot be adsorbed on the surface of amorphous SiO₂. Therefore, the flotation recovery rate is equal to that of crystalline SiO₂ is not the chemical agent's effect. Rather, mechanical entrainment causes amorphous SiO₂ to enter the concentrate.

3.3.4. Chemical calculation analysis of flotation solution

According to literature records, DDA's acid dissociation and dissociation equilibrium constant are $10^{-10.63}$ and $10^{-3.36}$, respectively. The dissociation formula of amine is as follows:



Taking the DDA concentration of 4×10^{-4} mol/L in the experiment as the initial concentration, the critical pH of RNH₂(s) was calculated as 9.35. The concentration changes of other components are shown in Fig. 10.

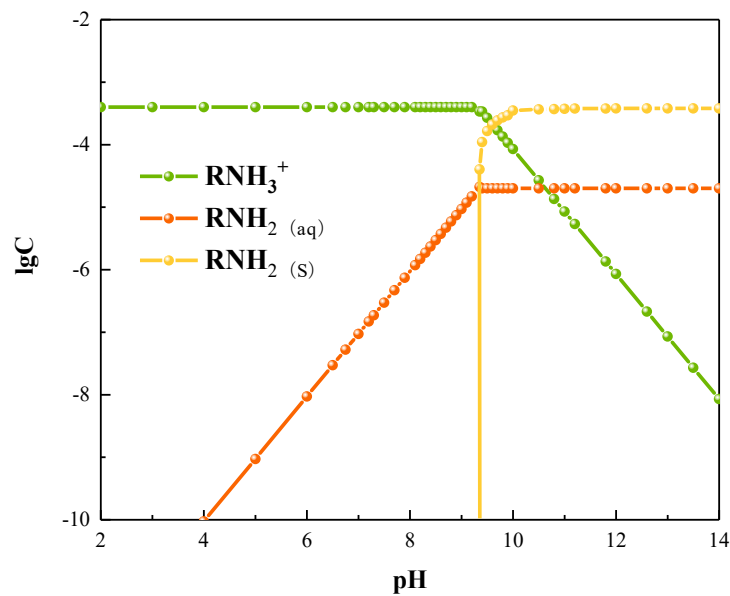


Fig. 10. Dodecylamine dissociation component diagram

After solution stoichiometry, it was found that when the pH was less than 9.35, the dissociated components of DDA were mainly RNH₃⁺, and the concentration of the components remained basically unchanged. With the increase in pH, the concentration of RNH₂(aq) component increased continuously until pH = 9.35. The RNH₂(s) component also appeared at pH = 9.35.

In the range of pH = 4–8, the DDA agent is mostly dissociated into cations. According to the Zeta potential test results, the isoelectric point (PZC) of the two SiO₂ species is about 2, and the SiO₂ surface is negatively charged at this time. Therefore, DDA is adsorbed on the surface of SiO₂ by electrostatic force. It is documented in the literature (Lu et al., 2016) that within this pH range, the dissociated RNH₃⁺ and RNH₂(aq) of DDA exist in the form of molecular associations, which does not conflict with the statement that RNH₃⁺ and RNH₂(aq) coexist. But combined with the results in this flotation experiment. Under the condition of acidic pulp, the flotation recovery rate was significantly increased. The

dissociation component diagram shows no significant change in the concentration of RNH_3^+ , so it is more likely that RNH_3^+ and $\text{RNH}_2(\text{aq})$ act synergistically (28).

When the pH exceeds pKa, the DDA agent mainly exists in the pulp solution in the form of DDA molecules. DDA cannot be adsorbed on the surface of SiO_2 minerals, thus resulting in a decrease in flotation recovery. According to flotation solution chemistry calculation, the flotation recovery should decrease after pH=9.35. In actual flotation, crystalline SiO_2 decreases at pH=7, and amorphous SiO_2 decreases at pH=8. Because DDA also forms ionic molecular dimer in solution, it can improve the adsorption of the agent on the SiO_2 surface. It exists a certain floating interval, which may be an important reason for the change of the optimal collection point (Gao et al., 2017; Yin and Sun, 2021). In addition, viscosity is also an important reason affecting the change of flotation recovery.

3.3.5. Surface tension analysis

The surface tension of the solution is a very important control parameter in flotation, which directly affects the flotation recovery rate of minerals. The surface tension of the collector DDA at 4×10^{-4} mol/L concentration was tested, and the results are shown in Fig. 11.

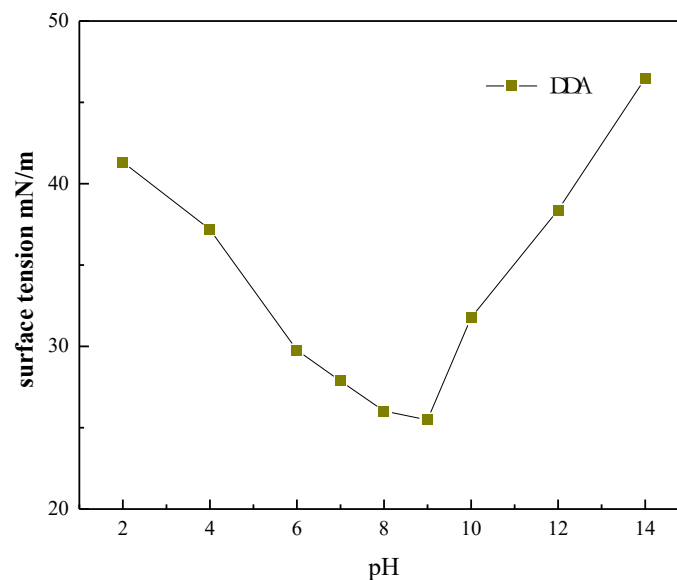


Fig. 11. Surface tension of solutions at different pH

As can be seen from the Fig., the surface tension is minimum at pH= 9, which is more conducive to flotation. This is not consistent with the optimal pH in actual flotation. According to Shen (2012) Colloid and surface chemistry, the surface tension is inversely proportional to the viscosity for DDA. It is further explained that the existence of viscous resistance changes the optimal pH in actual flotation.

3.3.6. DLVO theoretical analysis

In the classical theory of DLVO, it is believed that there are two interaction forces between charged colloidal particles, namely the electrostatic repulsion when the electric double layers overlap and the long-range van der Waals attraction between the particles (Cheng et al., 2020). In the absence of collectors, the two SiO_2 slurry colloid solutions only consider the existence of electrostatic force and van der Waals force, so they conform to the classical DLVO theory. The total action energy can be expressed as:

$$V_T^D = V_{ER} + V_{WA} \quad (3)$$

In the formula, V_T is the total potential energy of the slurry system, V_{ER} is the electrostatic interaction potential energy, and V_{WA} is the van der Waals interaction potential energy.

(1) Calculation of van der Waals potential energy

Assuming that the mineral particles of SiO₂ selected in the flotation experiment are consistent, SiO₂ with equal particle size can be calculated using the spherical interaction model. The simplified calculation formula is as follows:

$$V_{WA} = \frac{-AR}{12H} \quad (4)$$

$$A_{131} \approx (\sqrt{A_{11}} - \sqrt{A_{33}})^2 \quad (5)$$

In the formula, A is the Hamaker constant, R is the particle radius (nm), and H is the interaction distance (nm).

According to the available literature, the Hamaker constant of crystalline SiO₂ in vacuum is 6.35×10^{-20} J, and the Hamaker constant of amorphous SiO₂ in a vacuum is 9.6×10^{-20} J (or 15×10^{-20} J) (Himenez and Rajagopalan, 1997). Therefore, the Hamaker constants in the aqueous medium are 0.519×10^{-20} J and 1.098×10^{-20} J, respectively. The potential energy diagram of the van der Waals force can be drawn from this. As shown in Fig. 12.

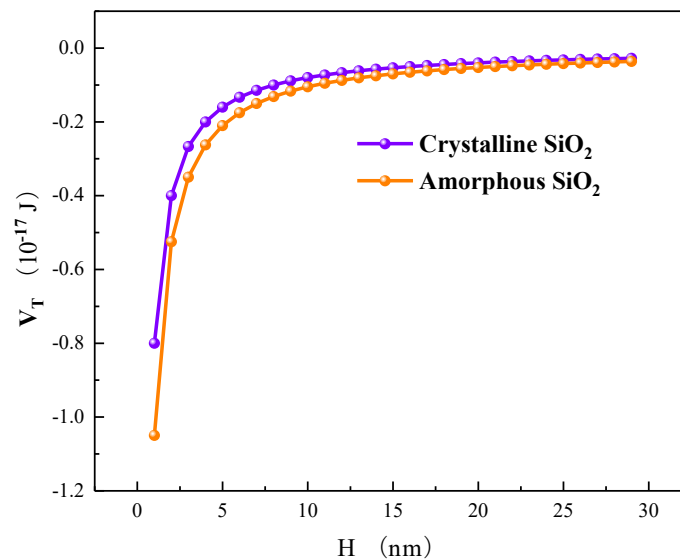


Fig. 12. Van der Waals action potential energy curve.

The Hamaker constant, seen from a microscopic perspective, is the dominant influence on the van der Waals interaction potential energy of the two SiO₂. The van der Waals potential energy of crystalline SiO₂ is higher due to the difference in van der Waals potential energy between the two crystal forms. From a macroscopic point of view, when the interaction distance between particles is smaller, the difference between the two is greater; that is, when the slurry concentration is higher, the van der Waals potential energy of crystalline SiO₂ is greater than that of amorphous SiO₂.

(2) Calculation of electrostatic interaction potential energy

From the zeta potential test results, it can be known that the surface of SiO₂ is negatively charged, and the electrostatic interaction force acts as a repulsive force. The calculation formula of electrostatic potential energy is as follows:

$$V_E = 2\pi\epsilon_0\epsilon_r R\phi^2 \ln(1 + e^{-\kappa H}) \quad (6)$$

$$\kappa = 0.568 \times 10^{10} \sqrt{C} \quad (7)$$

where κ is the Debye length, representing the thickness of the electric double layer; ϵ_0 is the absolute dielectric constant in vacuum, 8.854×10^{-12} F/m; ϵ_r is the dielectric constant of the dispersion medium; 78.5 F/m, ϕ is the particle surface potential; C is the electrolyte concentration. In the calculation process, the mineral surface potential ψ can be approximated by the potentiodynamic potential, namely the Zeta potential. At pH = 7, the potentiodynamic of crystalline SiO₂ and amorphous SiO₂ are -49.58 mV and -40.35 mV, respectively (Ding, 2010).

Finally, through calculation, at pH = 7, the electrostatic interaction potential energy curve of the two SiO₂ minerals at 20 μ m is shown in Fig. 13.

The classical DLVO theory cannot explain the system under flotation reagents. However, it can be explained by EDLVO theory. Hydration repulsion energy and hydrophobic interaction energy are taken into account based on van der Waals interaction and electrostatic interaction. DDA and SiO₂ play a part in the generated hydrophobic interaction in this system. Only the hydrophobic interaction energy needs to be considered when comparing the two. The calculation formula is as follows:

$$V_{HA} = \pi R h_0 V_{HA}^0 \exp\left(-\frac{H}{h_0}\right) \quad (8)$$

where R is the radius of spherical particles, nm; h₀ is the attenuation length, which is 10 nm; H is the interaction distance, nm; V_{HA}⁰ is -2 mJ/m². The hydrophobic interaction energy was calculated from this. The final total action potential energy curve is obtained by comprehensive DLVO theoretical calculation, as shown in Fig. 14.

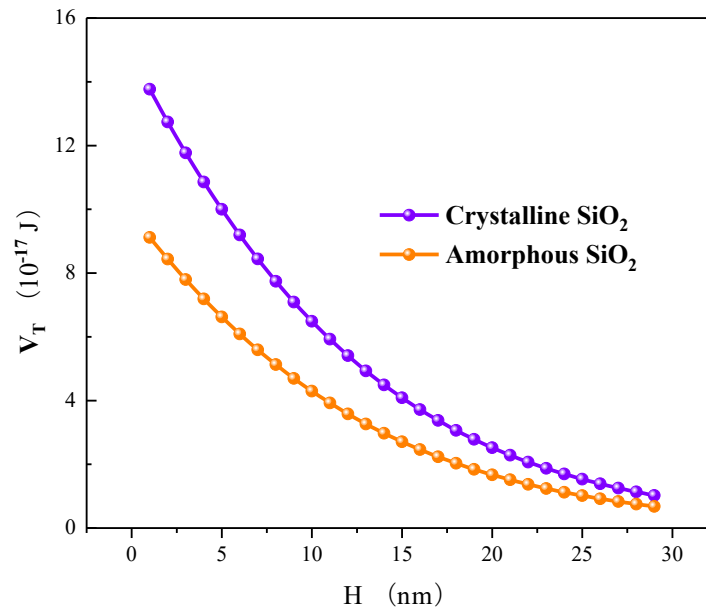


Fig. 13. Electrostatic interaction potential energy curve

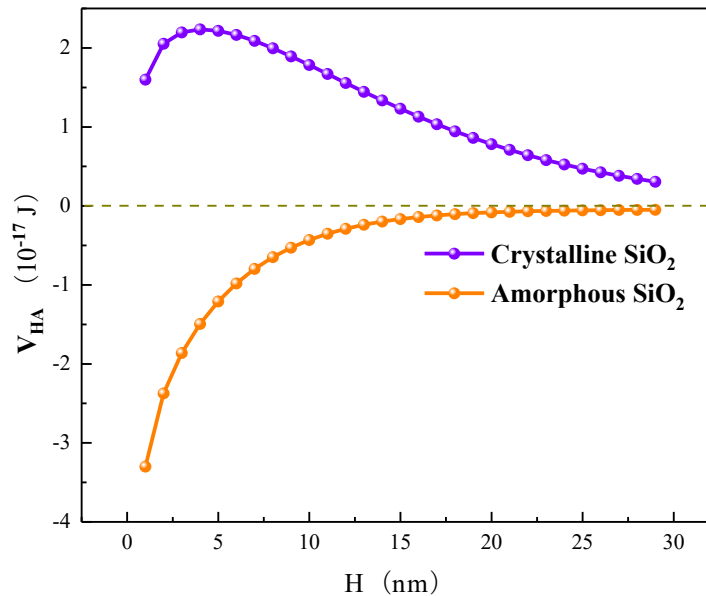


Fig. 14. Total action potential energy curve

According to studies on the explanation of colloidal coagulation, particles must overcome certain potential barriers to aggregate with each other. In general, the value is between 15 and 20 kJ/mol. In this verification calculation result, the total potential energy of classical DLVO is less than the above

range. The two SiO₂ particles in the sol system interact electrostatically, repelling one another, which is insufficient to break through the potential barrier. The hydrophobic interaction potential influences the total interaction potential of amorphous SiO₂, which results in agglomeration between particles when DDA is added to the solution. The total action potential energy of crystalline SiO₂ is positive, which shows that the particles repel each other. Therefore, it can be predicted that when the slurry concentration reaches a certain threshold, the interaction distance between particles decreases, and the electrostatic interaction between particles is relatively weakened. The aggregation tendency of amorphous SiO₂ particles is greater than that of crystalline SiO₂ (Wang et al., 2022). Especially in the aeration process of flotation, the mutual cohesion of the amorphous SiO₂ particles will be more serious. Eventually, the amorphous SiO₂ particles of the unadsorbed agent will float together with the particles of the adsorbed agent (Liang, 2018).

Conclusions

- (1) The flotation results show that in the study of reagent concentration, crystalline SiO₂ is more sensitive to the feedback of the change of reagent concentration. Crystalline SiO₂ requires lower concentrations of reagents to achieve optimal flotation recovery.
- (2) From the comprehensive analysis of the experimental results of adsorption content and the semi-quantitative calculation results of the infrared spectrum, it can be concluded that there is a significant difference in the adsorption amount between the two. Adsorbent is more concentrated on the surface of crystalline SiO₂ than amorphous SiO₂, with a difference of around 23%.
- (3) Zeta potential and DLVO theoretical calculations show that due to the surface inhomogeneity of amorphous SiO₂, the stability of the slurry system is lower than that of crystalline SiO₂ resulting in stronger hydrophilic ability. In the flotation process, the agglomeration tendency of amorphous SiO₂ is stronger under the same agent concentration.
- (4) Amorphous SiO₂ will increase the difficulty of flotation due to the difference in its surface properties. Mechanical entrainment will occur throughout the flotation process and will enter the concentrate with the foam. Therefore, it is crucial to identify the crystal form of SiO₂ in the mineral during beneficiation in order to prepare it for further flotation.

Acknowledge

The study received funding supported from the National Natural Science Foundation of China (Grant No.51764045), Science and Technology program of Baotou City of China (Grant No:2019Z3004-5), Inner Mongolia Autonomous Region Science and Technology plan Project (Grant No.2021GG0438) and Inner Mongolia Natural Science Foundation (2020MS05048, 2020BS05029).

References

- ABBAKER, A., ASLAN, N., 2023. *The effect of microbubbles on coarse particle anionic flotation: analysis and optimization*. Physicochem. Probl. Miner. Process. 59(6), 172298.
- BERRO, Y., BADAWI, M., EL HAJ HASSAN, F., KASSIR, M., TIELENS, F., 2020. *Water-silanol interactions on the amorphous silica surface: A dispersion-corrected DFT investigation*, J. Mol. Liq. 320, 114496.
- CAO, S., YIN, W., YANG, B., ZHU, Z., SUN, H., SHENG, Q., 2021. *Insights into the influence of temperature on the adsorption behavior of sodium oleate and its response to flotation of quartz*, International Journal of Mining Science and Technology, 32(2), 399-409.
- CHEN, X., HADDE, E., LIU, S., PENG, Y., 2017. *The effect of amorphous silica on pulp rheology and copper flotation*, Miner. Eng., 113. 41-46.
- CHENG, H., WANG, H., HUANG, G., YANG, W., XU, T., ZHAO, J., 2020. *Model and Verification of Clay Particle Separation Ability and Liquid-Solid Ratio Based on DLVO Theory*, Journal Nanchang Institute of Technology, 39, 38-43
- DING, Y., 2010. *Study on the preparation of high-purity quartz from low-grade quartz ore*, Northeastern University, p. 164
- GAO, Y., GAO, Z., SUN, W., 2017., *Effect of metal ions mineral flotation behavior and mechanism research progress*. China Nonferrous Gold Acta Petrolei Sinica. 27(04), 859-868.

- GRIFFITHS, P.R., DE HASETH, J.A., 2006. *Fourier Transform Infrared Spectrometry*, John Wiley & Sons, Inc.
- HIEMENZ, P.C., RAJAGOPALAN, R., 1997. *Principles of Colloid and Surface Chemistry*, Third Edition, Revised and Expanded, Taylor and Francis; CRC Press.
- HU, P., LI, Q., LI, L., 2021. *A review of characterization techniques of heterocoagulation between mineral particles in mineral separation process*, Sep. Purif. Technol., 279, 119699.
- HU, X., LI, G., SUN, M., HU, H., 2007. *Crystal shape and particle size distribution control of silica powder used as raw material for quartz glass*. China non-metallic mineral industry guide, 04, 41-43.
- HU, Y., LIN, Y., 1990. *Flotation solution chemistry*, Metal ore beneficiation abroad, 1-7
- LELIS, D.F., FERNANDES LIMA, R.M., ROCHA, G.M., LEÃO, V.A., 2022. *Effect of Magnesium Species on Cationic Flotation of Quartz from Hematite*, Min. Proc. Ext. Met. Rev. 43, 339-345.
- LI, J., LIU, J., SUN, J., LI, X., ZHAO, J., GUO, X., 2021. *Study on the Purification Effect of Amorphous Microsilica Fume by Flotation Method*, Coal Preparation Technology, 136-141.
- LIU, Y., TONG, X., XIE, R., XIAN, X., SONG, Q., FAN, P., 2023. *Activation of quartz flotation by Cu^{2+} , Ni^{2+} in the sodium ethylxanthogenate (EX) system*. Physicochem. Probl. Miner. Process. 59(2), 166368.
- LIANG, L., 2018. *Study on selective aggregation mechanism of clay minerals in slime*, CUMT.
- LIU, W., WANG, X., PENG, X., DUAN, H., 2010. *A spectrophotometric method for the detection of amine collectors*, 201811226293[P]
- LIU, Y., GONG, H., ZHANG, K., 1992. *Adsorption mechanism of dodecylamine hydrochloride on feldspar quartz surface and effect of PH value on adsorption*. China Mining Industry, 02, 92-96.
- LU, J., GAO, H., JIN, J., CEN, D., REN, Z., 2016. *Influence and mechanism of calcium ions on andalusite flotation*, Chinese Journal of Nonferrous Metals 26, 1311-1315.
- MARTÍNEZ-CARRILLO, D., URIBE-SALAS, A., 2018. *An experimental study of the recovery of hydrophilic silica fines in column flotation*, Miner. Eng. 21, 1102-1108.
- MI, H., CHEN, Y., GAO, S., LIU, W., CHENG, H., 2018. *Study on the relative wettability of fine-grained quartz and its flotation behavior*, Mineral Conservation and Utilization, 93-99.
- NYKÄNEN, V.P.S., BRAGA, A.S., PINTO, T.C.S., MATAI, P.H.L.S., LIMA, N.P., LEAL FILHO, L.S., MONTE, M.B.M., 2020. *True flotation versus entrainment in reverse cationic flotation for the concentration of iron ore at industrial scale*, Min. Proc. Ext. Met. Rev. 41, 11-21.
- SHEN, Z., 2012. *Colloid and surface chemistry*. Chemical Industry press 2012.
- SHI, T., ZHANG, T., 2017. *Effects of crystal structure and surface properties on quartz flotation behavior*, Acta Minera Sinica 37, 333-341.
- WANG, D., 1988. *Flotation Solution Chemistry*,
- WANG, Y., LI, J., ZHANG, W., LI, P., GUO, J., YAO, K., 2021. *Citric acid inhibits the floatability of quartz in Mg^{2+} system*, Physicochem. Probl. Miner. Process., 57(6), 1-11.
- WANG, L., LI, M., ZOU, Y., 2023. *Rheological properties and entrainment behavior of crystalline/amorphous silica in chalcopyrite flotation system*, Journal of Engineering science, 45, 1272-1280.
- WANG, G., SHUI, M., YUE, L., 2002. *X-ray diffraction analysis of the structure and physicochemical properties of amorphous silica*, Chinese Journal of Inorganic Chemistry, 991-996.
- WEI, P., REN, L., HANG, Q., FANG, Z., 2018. *Influence of cationic collectors on quartz fractionation flotation behavior*, Mining and Metallurgical Engineering 38, 64-67.
- WENG, S., 2010. *Fourier transform infrared spectroscopy*, Chemical Industry Press Pub., ISBN 10: 7122076385
- WU, J., LI, J., LIN, J., YI, S., LI, M., SU, W., 2021. *Infrared Fitting Spectral Analysis of Influence Mechanism of Microwave on Barite Flotation*, Spectroscopy and Spectral Analysis 41, 3083-3091.
- YE, J., WANG, X., 2018. *Effect of dispersants on dispersion stability of collophane and quartz fines in aqueous suspensions*, J. Disper. Technol. 39, 1655-1663.
- YIN, W., SUN, C., 2021. *Research status of Silicate mineral flotation principle*. Mineral protection and Utilization, 03, 17-22.
- ZHOU, K., 2015, *Research on Quartz Surface Properties and Flotation*, Guizhou University, p. 69
- ZHOU, Q., WEI, J., ZHU, J., ZHU, R., TANG, C., HE, H., 2015. *Computational simulation of differences in surface structure and hydration characteristics of silica homogeneous polymorphic minerals*, The 15th Annual Conference of the Chinese Society of Mineralogy, Petrology and Geochemistry, China Changchun, Jilin, 3-44
- ZHU, Z., YIN, W., WANG, D., SUN, H., CHEN, K., YANG, B., 2020. *The role of surface roughness in the wettability and floatability of quartz particles*, Appl. Surf. Sci. 527, 146799.